

Impact of Microscale and Pilot-Scale Freeze-Drying on Protein Secondary Structures: Sucrose Formulations of Lysozyme and Catalase

BJÖRN-HENDRIK PETERS,¹ JARI T.T. LESKINEN,² FERDINAND MOLNÁR,¹ JARKKO KETOLAINEN¹

¹University of Eastern Finland, School of Pharmacy, Kuopio, Finland

²University of Eastern Finland, SIB Labs, Kuopio, Finland

Received 7 May 2015; revised 28 July 2015; accepted 4 August 2015

Published online in Wiley Online Library (wileyonlinelibrary.com). DOI 10.1002/jps.24615

ABSTRACT: Microscale (MS) freeze-drying offers rapid process cycles for early-stage formulation development. The effects of the MS approach on the secondary structures of two model proteins, lysozyme and catalase, were compared with pilot-scale (PS) vial freeze-drying. The secondary structures were assessed by attenuated total reflection Fourier transformed infrared spectroscopy. Formulations were made with increasing sucrose–protein ratios. Freeze-drying protocols involved regular cooling without thermal treatment and annealing with MS and PS equipment, and cooling rate variations with the MS. Principal component analysis of smoothed second-derivative amide I spectra revealed sucrose–protein ratio-dependent shifts toward α -helical structures. Transferability of sucrose–protein formulations from MS to PS vial freeze-drying was evidenced at regular cooling rates. Local differences in protein secondary structures between the bottom and top of sucrose–catalase samples could be detected at the sucrose–catalase ratios of 1 and 2, this being related to the initial filling height and ice crystal morphology. Annealing revealed temperature, protein, formulation, and sample location-dependent effects influencing surface morphology at the top, or causing protein secondary structure perturbation at the bottom. With the MS approach, protein secondary structure differences at different cooling rates could be detected for sucrose–lysozyme samples at the sucrose–lysozyme ratio of 1. © 2015 Wiley Periodicals, Inc. and the American Pharmacists Association *J Pharm Sci*

Keywords: freeze-drying; lyophilization; FTIR; calorimetry (DSC); multivariate analysis; principal component analysis; proteins; protein formulation

INTRODUCTION

Freeze-drying is a common biopharmaceutical manufacturing procedure intended to ensure product quality during shipment and storage.¹ Despite extensive efforts made by the freeze-drying community, formulation development often remains a time-consuming, trial-and-error process.² Various approaches have been described in attempts to solve these problems, for example, utilizing downscaled well-plate setups in connection with screening of stabilizers³ or visual cake quality assessment by high-throughput screening.⁴ Recently, a microscale (MS) setup based on the heating stage of a freeze-drying microscope was claimed to achieve a drastically reduced process cycle time.⁵ Although good agreement has been detected between nucleation temperature (T_n) and pore morphology with vial freeze-drying,⁵ there are nonetheless substantial differences with regards to heat transfer, sample holder, and achievable cooling rates. Most importantly, it remains to be demon-

strated if protein formulations freeze-dried with this type of MS setup are qualitatively equivalent to those prepared by a vial freeze-drying process; this is clearly a prerequisite for scale up. At present, scale-up to vial freeze-drying has been conducted for lactate dehydrogenase³ and granulocyte colony-stimulating factor (G-CSF)⁶ utilizing a downscaled well-plate setup. Nevertheless, in both of these studies, the retention of biological activity, which was assessed immediately after freeze-drying, was the sole indicator of a successful formulation and its transferability.^{3,6} Although the presence of biological activity is without question of major importance for a satisfactory product, it may not be possible to conclude from this property on its own that protein secondary structures were preserved similarly in the freeze-dried solid at both processes. For example, during reconstitution, processing stresses that altered a protein's active conformation could be masked because of refolding of the partially unfolded protein back into its active conformation, as has been reported for lysozyme, α -lactalbumin, and chymotrypsinogen.^{7,8} In contrast to the general assumption that structural perturbations tend to occur during the dehydration event, for G-CSF, only a minor conformational change was noted at pH 7.5.⁹ The quality by design initiative¹⁰ emphasizes that an awareness of the equivalence of one critical quality attribute of the final product alone is not sufficient for guaranteeing successful formulation development, transfer, and scale-up; this caveat is especially true for protein-based products that have such diverse and complex behaviors.

Fourier transformed infrared (FTIR) spectroscopy represents one possibility to gain further process understanding. FTIR has been routinely used to investigate freeze-dried

Abbreviations used: AN 10, annealing/annealed at -10°C ; AN 20, annealing/annealed at -20°C ; AO, area of overlap; ATR, attenuated total reflection; CR 1, cooling rate of $1^\circ\text{C}/\text{min}$; DSC, differential scanning calorimetry; FTIR, Fourier transformed infrared; G-CSF, granulocyte colony-stimulating factor; MS, microscale; PC, principal component; PCA, principal component analysis; PS, pilot scale; SEM, scanning electron microscopy; SIMCA, soft independent modeling of class analogy; T_g' , glass transition temperature of the maximally freeze-concentrated solution; T_n , nucleation temperature.

Correspondence to: Björn-Hendrik Peters (Telephone: +358-50-59-44-55-3; Fax: +358-17-162-424; E-mail: bjorn.peters@uef.fi)

This article contains supplementary material available from the authors upon request or via the Internet at <http://wileyonlinelibrary.com>.

Journal of Pharmaceutical Sciences

© 2015 Wiley Periodicals, Inc. and the American Pharmacists Association

samples in either the solid state after processing or in the liquid state after reconstitution. The amide I region, originating mainly from C-O stretch vibrations of the peptide linkages,^{11,12} is particularly interesting. The identification and semiquantitative comparison of protein secondary structures based on mathematical methods applied to the amide I region have been described by Dong et al.¹³ and Dong and Caughey.¹⁴ Recently, the DModXPS values of proteins in solution obtained by soft independent modeling of class analogy (SIMCA) were shown to provide a sensitive quantitative indicator of changes in a protein's higher-order structure.¹⁵ To provide evidence that the MS approach could be utilized for early-stage formulation development, this present study investigates the formulation- and process-dependent variations in the secondary structure of two model proteins formulated either without a stabilizer or in sucrose, a disaccharide commonly utilized in freeze-drying,¹⁶ exploiting both MS and pilot-scale (PS) equipment. Furthermore, the feasibility of using the SIMCA methodology proposed by Stockdale et al.¹⁵ for solid-state FTIR-attenuated total reflection (ATR) measurements was evaluated.

MATERIALS AND METHODS

Sucrose (S7903) and bovine liver catalase (crystalline suspension, C30) were purchased from Sigma–Aldrich (St. Louis, Missouri). Hen egg white lysozyme was obtained from Dalian Greensnow Egg Products Development Company, Ltd. (Dalian City, China). Milli-Q-water (EMD Millipore, Billerica, Massachusetts) was produced immediately before use by filtration and used at all times. Concentrations were w/w unless stated otherwise.

MS Freeze-Drying

Microscale freeze-drying was performed on a THMS350V heating stage and controlled by the Linksys32 software package (both Linkam Scientific, Guildford, UK). Calibration of the temperature sensor and sample placement were performed as described earlier.⁵ Briefly, before sample placement, approximately 5 μL of silicon oil were dispensed onto the silver heating block followed by a cover glass #1 with a 15-mm diameter (Menzel GmbH, Braunschweig, Germany) acting as the vial bottom that would be present in vial freeze-drying. The vial side wall was replaced by an in-house manufactured cylindrical, hollow polypropylene sample holder. A volume of 200 μL of sample was pipetted into this assembly, cooled down to -50°C at a rate of $10^\circ\text{C}/\text{min}$, held at this temperature for 8 min, and then dried at -33°C for 75 min. For certain formulations, this protocol was adapted to include either an intermediate annealing step of 30 min or a cooling rate of $1^\circ\text{C}/\text{min}$ (CR 1) that consisted of cooling the sample down to -25°C at a rate of $1^\circ\text{C}/\text{min}$ followed by cooling down to -50°C at a rate of $10^\circ\text{C}/\text{min}$. After primary drying, the sample was heated to 30°C as described earlier⁵ and held at this temperature for 5 min. No stoppering device was used. Subsequently, the samples were transferred into a desiccator for intermediate storage prior to their assessment. The T_n was noted down as the silver heating block temperature at visual observation of the nucleation event.

PS Freeze-Drying

Pilot scale freeze-drying was performed in a Lyostar II FTS (SP Scientific, Warminster, Pennsylvania). The formulations were

filled into 2 mL Fiolax Clear vials (Schott AG, Mainz, Germany) in volumes of 1 mL per vial and these were placed in the center of the tray. Vials containing samples for biological activity assessment were half stoppered with 13 mm Freeze Dry Stoppers 4023/50 (Adelphi Healthcare Packaging, Haywards Heath, UK). Vials containing samples for FTIR-ATR and scanning electron microscopy (SEM) assessment were cut at the top prior to freeze-drying to permit release of the intact freeze-dried cake later; these vials were not stoppered. Vials were surrounded by three rows of dummy vials filled with water to reduce edge vial effects. The samples were cooled down to -45°C at a rate of $1^\circ\text{C}/\text{min}$, held at this temperature for 2 h, followed by primary drying at -33°C . The endpoint of primary drying was considered to have occurred when identical pressure readings from the Pirani gauge and capacitance manometer were obtained. An intermediate annealing step of 10 h was included for certain formulations. After the primary drying, samples were heated to 25°C at a rate of $0.2^\circ\text{C}/\text{min}$ and held at this temperature for 2 h. The chamber pressure difference between MS and PS at equal pressure set points of 80 mTorr was a maximum of 46 mTorr (Pirani gauge readings) because of technical limitations. Subsequently, the samples were transferred into a desiccator for intermediate storage prior to their assessment.

Differential Scanning Calorimetry

Differential scanning calorimetry (DSC) was performed with a DSC 823e (Mettler-Toledo GmbH, Greifensee, Switzerland). The heating cell was calibrated using water, indium, lead, and zinc under a nitrogen flow of 50 mL/min. A sample volume of 30 μL was pipetted into an aluminum crucible and hermetically sealed. Samples were cooled down from 20°C to -70°C at a rate of $10^\circ\text{C}/\text{min}$, held at this temperature for 10 min, and then heated to 20°C at a rate of $5^\circ\text{C}/\text{min}$.

FTIR-ATR Assessment

Fourier transformed infrared-ATR spectroscopy was used for the analysis of the protein secondary structures present in the freeze-dried cakes. The assessment was performed with a Nicolet 8700 spectrometer (Thermo Fisher Scientific, Madison, Wisconsin) equipped with a Smart Endurance ATR stage and a DTGS detector. The stage was continuously purged with dry nitrogen to remove any detectable carbon dioxide and water vapor. The background was measured at identical settings and automatically subtracted from the subsequent measurements. Samples were released from the primary packaging container directly onto the sample stage, fixed, and measured without further preparation. Each sample was measured 256 times at a resolution of 2 cm^{-1} between 4000 and 650 cm^{-1} at the bottom and the top. For each model formulation, three samples were prepared ($n = 3$). The residual moisture content of the samples was measured using a KF C30 coulometer (Mettler-Toledo GmbH) and was found to be less than 0.5% (v/v).

The terms “bottom” and “top” utilized throughout this report require some clarification in order to avoid potential misunderstandings. Originally, sample preparation prior to FTIR measurements in transmission mode involved grinding of the lyophile with potassium bromide and subsequent compression into a pellet under vacuum.¹⁷ This procedure had been claimed not to cause significant alterations in the protein–disaccharide interactions¹⁸ and to produce only minor, if any, effects on protein secondary structures.^{19,20} However, this meant that only

a putatively representative sample portion could be measured. This method differs for FTIR-ATR measurements where sample preparation involves the removal of the sample from its holder, placement of the lyophile on top of the measurement crystal, and fixation of the sample. Therefore, in this report, “bottom” refers to a freeze-dried sample placed onto the measurement crystal in accordance with its orientation in the sample holder and “top” describes a freeze-dried sample inverted by 180° along its horizontal axis before being placed onto the measurement crystal. Furthermore, the results presented as “bottom” and “top” are assumed to refer to a sample portion, not exclusively to the outermost layer of the sample. Such an assumption is reasonable and takes into account the FTIR-ATR beam penetration depth²⁰ and the porosity of freeze-dried samples,⁵ potentially causing intermediate layers to fill the voids of the outermost layer during fixation.

Spectral Processing and Analysis

Second derivatives of the amide I region (1700 to 1600 cm⁻¹) were calculated following Savitzky–Golay smoothing with a nine-point third-order polynomial using the OMNIC software package (Thermo Fisher Scientific) and area normalized with an in-house MATLAB® (The MathWorks, Natick, Massachusetts) routine. Then, the area of overlap (AO) was calculated according to the procedure described by Kendrick et al.²¹ With respect to AO calculation and to facilitate the MS to PS comparison, the spectra of the first PS sucrose–protein sample of the highest ratio were used as reference.

An extensive introduction to the SIMCA approach can be found in Stockdale et al.¹⁵ In brief, SIMCA-P+ (Umetrics AB, Umeå, Sweden) was used for principal component analysis (PCA) of the area-normalized and mean-centered spectra in order to qualitatively analyze the sucrose concentration and process cycle-dependent protein secondary structure variations. Then, SIMCA modeling was performed with the same software to construct PCA models for appropriate sample groups. Subsequently, the model sample groups, one at a time, were compared with other samples to obtain a measure of distance from the respective sample group, that is, the descriptor DModXPS. The D-Crit value was calculated based on an α -value of 0.001. A DModXPS-value higher than D-Crit indicated with a probability of 99.9% that a sample is not a member of the sample group originally used to create the model. Finally, in order to confirm that the DModXPS descriptor could be used reliably as a quantitative surrogate in this solid-state FTIR-ATR approach, the correlation with AO was calculated.

Bands identified in the loading (PCA) or contribution (SIMCA) plot were interpreted in accordance with Dong et al.¹³ and Dong and Caughey.¹⁴

Scanning Electron Microscopy

The freeze-dried samples were coated using an Agar Auto Sputter Coater (Model B7341; Agar Scientific Ltd., Stansted, UK) in order to ensure electric conductivity on the sample surfaces and to minimize or eliminate surface charging. A sputter time of 120 s and a gold anode were used, resulting in a coating thickness of approximately 60–70 nm. Subsequently, morphology and thickness were observed with a Field Emission (Schottky type) SEM (Carl Zeiss Sigma HD VP; Carl Zeiss NTS, Cambridge, UK). During the observation, an acceleration voltage of 6 kV combined with an aperture of 30 μ in diameter was

used under high vacuum conditions (pressure, $P < 2$ mPa). The micrographs were captured with an Everhart–Thornley type secondary electron detector with 300 V grid bias in order to gain surface topographic contrast.

Fluorescence-Based Biological Activity Assay

The biological activity of lysozyme was assessed with the EnzoChek Lysozyme Assay Kit (E-22013; Thermo Fisher Scientific) as described earlier.⁵ The biological activity of catalase was assessed with the Amplex® Red Catalase Assay Kit (Thermo Fisher Scientific) according to the manufacturer’s recommendations. Freeze-dried samples were reconstituted with water to the original sample volume and diluted down to a concentration of 6.25 μ g/mL using a 0.1-M Tris–HCl pH 7.5 reaction buffer. For each reaction, 25 μ L of the diluted sample and 25 μ L of 40 μ M hydrogen peroxide solution were pipetted into the well of a 96-well ViewPlate (PerkinElmer, Waltham, Massachusetts). After incubation of the samples for 30 min at room temperature, 50 μ L of 10 μ M Amplex® Red and 40 μ M horseradish peroxidase mixture were added to each well and the samples were incubated for 30 min at 37°C in the dark. The fluorescence intensity of each reaction was measured in an EnVision 2004 multilabel reader (PerkinElmer) equipped with monochromators set to excitation at 545 nm and emission at 590 nm.

RESULTS

Lysozyme Formulations

The results originating from FTIR-ATR lysozyme sample spectra are presented in Figure 1. Representative spectra of each formulation prepared at PS are presented in Figure 1a to provide an overview of how changes in the sucrose–lysozyme ratio were related to protein secondary structure variation. A clear shift of the most intense peak from approximately 1641 to approximately 1652 cm⁻¹ was noted with increasing sucrose–lysozyme ratios. The PCA score plot including all spectra is presented in Figure 1b. Principal components (PCs) 1 and 2 accounted for 94% (PC 1: 83%, PC 2: 10%) of the dataset variation. One spectrum of lysozyme without sucrose was proposed as an outlier (Hotelling’s T² 95%, gray-colored square in Fig. 1b) but was kept as a part of the model. The visual inspection of the score plot identified three distinct groups, separated according to their sucrose contents. Furthermore, a clear shift from the right to the left along PC 1 was found and this corresponded to the increase in the sucrose–lysozyme ratio from 0 to 1. The loading plot (Fig. 1c) to Figure 1b explained this shift along PC 1 as being a change from predominantly β -sheet (1615, 1641, 1689 cm⁻¹) to α -helical (1654 cm⁻¹), β -sheet (1623 cm⁻¹), and β -turn (1667 cm⁻¹) structures. The DModXPS results are depicted in Figure 2. The DModXPS descriptor was calculated for all spectra based on a SIMCA model created from PS sucrose 1% sample spectra (model samples shown as red bars in Fig. 2). At the sucrose–lysozyme ratio of 1, all regular MS and MS CR 1 bottom and top samples were similar but did not belong to the model sample group. Similarly, MS AN 10 (annealed at –10°C) bottom samples were close, whereas one out of three MS AN 10 top samples was found to belong to the model sample group. Importantly, the correlation between DModXPS and AO (Fig. 1d) was found to be excellent, that is, correlation coefficient $R^2 = 0.9467$.

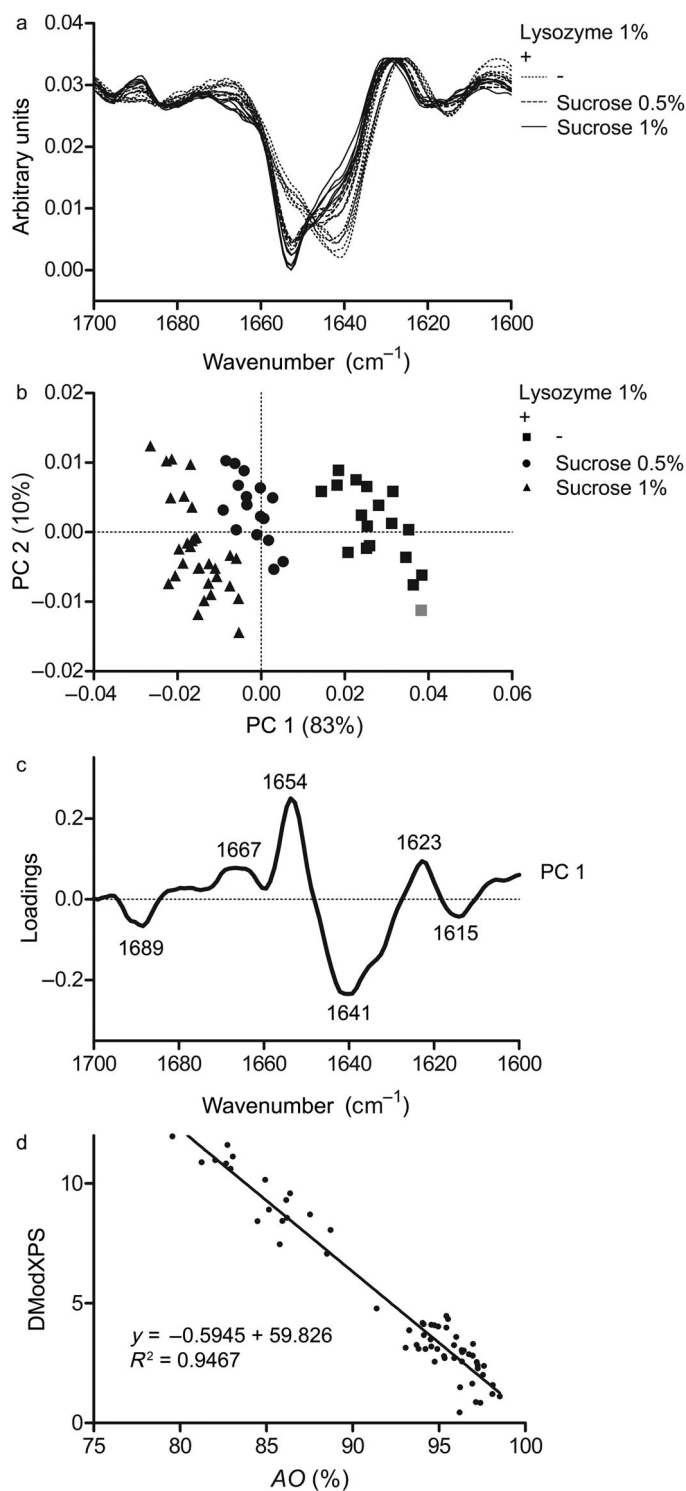


Figure 1. (a) Fourier transformed infrared-ATR spectra of PS lysozyme samples. (b) PCA score plot of all FTIR-ATR lysozyme spectra (the gray square was proposed as outlier but kept in the model). (c) PCA loading plot of PC 1 to (b). (d) Correlation plot between AO and DModXPS.

The AO results are summarized in Table 1. For lysozyme without sucrose the AO varied between approximately 83%–86%. At a sucrose–lysozyme ratio of 0.5, the AO increased to approximately 94%–95% and achieved approximately 94%–98% at a ratio of 1. For a few sucrose 1% samples, a tendency to-

ward greater AO at the top was noted when comparing bottom and top against their respective references (Table 1, columns “Bottom Versus Bottom” and “Top Versus Top”). Nevertheless, no significant difference between bottom and top was found with the SIMCA model created from the MS and PS sucrose 1% bottom sample spectra (not shown). Furthermore, for the sucrose 1% formulations, the MS CR 1 samples showed an increased AO when compared with the respective regular MS samples at both bottom and top. The results of the SIMCA model created from these regular MS samples are presented in Figure 3. Representative FTIR-ATR spectra of regular MS and MS CR 1 samples are shown in Figure 3a and provide an overview of how changes in the MS cooling rate were related to protein secondary structure variation. Although the peak intensity difference of the α -helical peak at approximately 1654 cm^{-1} was clearly seen and initially considered to be the source of group separation depicted in Figure 3b (model samples shown as red bars), the contribution plot (Fig. 3c) identified the β -sheet structures at 1642 cm^{-1} as the major source of group separation.

All MS and PS samples revealed almost identical biological activities after reconstitution (not shown).

Catalase Formulations

The results originating from FTIR-ATR catalase sample spectra are presented in Figure 4. Representative spectra of each formulation prepared at PS are presented in Figure 4a to provide an overview of how changes in the sucrose–catalase ratio were related to protein secondary structure variation. A clear increase in α -helical peak intensity at approximately 1658 cm^{-1} and a shift of the β -sheet peak from approximately 1638 to approximately 1642 cm^{-1} was noted with increasing sucrose–catalase ratios. The PCA score plot including all spectra is presented in Figure 4b. PCs 1 and 2 accounted for 87% (PC 1: 81%, PC 2: 6%) of the dataset variation. The visual inspection of the score plot identified four distinct groups; three could be categorized according to the sucrose–catalase ratios, displaying a shift along PC 1 from right to left: catalase (1) without sucrose, (2) with sucrose 0.5%, (3) with sucrose 1% and 2%. The fourth group consisting of three 2% sucrose samples was located between groups (1) and (2) and identified as PS AN 10 bottom samples. The loading plot (Fig. 4c) to Figure 4b explained this shift along PC 1 as being a change from predominantly β -sheet (1615 and 1634 cm^{-1}) and disordered (1648 cm^{-1}) to α -helical (1658 cm^{-1}) and β -sheet (1642 and 1685 cm^{-1}) structures. The DModXPS results are depicted in Figure 5. The DModXPS descriptor was calculated for all spectra based on a SIMCA model created from PS sucrose 2% sample spectra (model samples shown as red bars in Fig. 5). At a sucrose–catalase ratio of 1, one out of three MS bottom samples and two out of three MS top samples were found to belong to the model sample group. Similarly, one out of three MS AN 20 (annealed at -20°C) bottom samples and all MS AN 20 top samples were found to belong to the model sample group.

In addition to the MS to PS comparison, all PS regular and PS AN 20 samples with sucrose–catalase ratios of 1 and 2 were found to belong to the model sample group. Catalase formulations annealed at -10°C either collapsed during the process (MS) or the bottom samples did not belong to the model sample group (both PS AN 10 sucrose 1% and PS AN 10 sucrose 2%), whereas the corresponding top samples were found to belong to

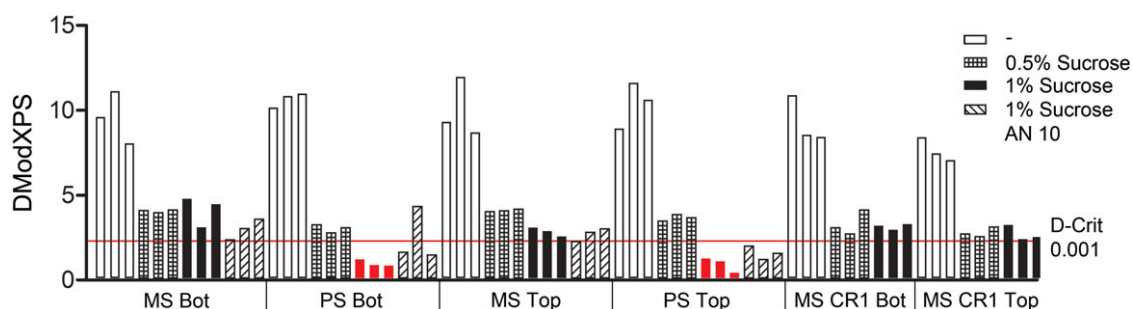


Figure 2. Lysozyme DModXPS distance plot based on the SIMCA-PCA model of PS samples prepared from 1% sucrose (all w/w; shown as red bars). (The reader is referred to the web version of this article for interpretation of the references to color in this figure legend).

Table 1. Area of Overlap Results of Freeze-Dried Model Protein Formulations

Formulation	Protocol	Scale	AO (%) ^a		
			Bottom Versus Bottom	Top Versus Top	
Lysozyme (1%) +					
–	Regular	MS	86.04 ± 2.85	84.40 ± 4.26	
		PS	83.20 ± 1.52	83.60 ± 1.34	
Sucrose (0.5%)	Regular	MS	84.45 ± 2.79	86.25 ± 2.06	
		PS	94.69 ± 0.67	94.58 ± 0.47	
Sucrose (1%)	Regular	MS	94.96 ± 0.89	94.90 ± 1.67	
		PS (Ref.)	97.27 ± 0.18	97.36 ± 1.65	
	CR 1	MS	95.95 ± 1.25	96.77 ± 0.78	
		AN 10	MS	96.64 ± 0.86	96.88 ± 0.41
		PS	96.22 ± 0.70	97.92 ± 0.32	
Catalase (1%) +					
–	Regular	MS	77.86 ± 0.91	77.54 ± 2.04	
		PS	76.75 ± 0.74	77.88 ± 0.95	
Sucrose (0.5%)	Regular	MS	89.68 ± 0.77	89.88 ± 1.37	
		PS	88.93 ± 0.48	91.69 ± 0.86	
Sucrose (1%)	Regular	MS	91.46 ± 0.36	93.62 ± 1.43	
		PS	93.29 ± 0.39	95.45 ± 0.25	
		AN 20	MS	91.50 ± 1.38	94.49 ± 0.67
	AN 10	PS	92.43 ± 0.34	94.31 ± 0.61	
		MS	–	–	
		PS	91.31 ± 0.60	93.70 ± 1.96	
Sucrose (2%)	Regular	PS (Ref.)	94.11 ± 0.56	95.98 ± 0.58	
		AN 20	PS	93.62 ± 1.13	94.67 ± 0.30
		AN 10	PS	86.54 ± 2.04	94.31 ± 0.61

^aReference samples for AO calculations were for the lysozyme formulations regular PS sample 1 of the 1% sucrose formulation and for the catalase formulations regular PS sample 1 of the 2% sucrose formulation.

AO, area of overlap; CR 1, cooling rate 1°C/min; AN 10, annealing at –10°C; AN 20, annealing at –20°C; MS, microscale; PS, pilot scale; Ref., reference formulation.

All formulation percentages reported as w/w; AO reported as mean ± SD, $n = 3$ (from reference formulations the first sample was used as reference, presented percentages were calculated based on the remaining samples, $n = 2$).

the model sample group. Results of an attempt to investigate the morphological behavior leading to collapse will be described later. Importantly, the correlation between the DModXPS descriptor and the AO (Fig. 4d) was found to be excellent, that is, correlation coefficient $R^2 = 0.9898$.

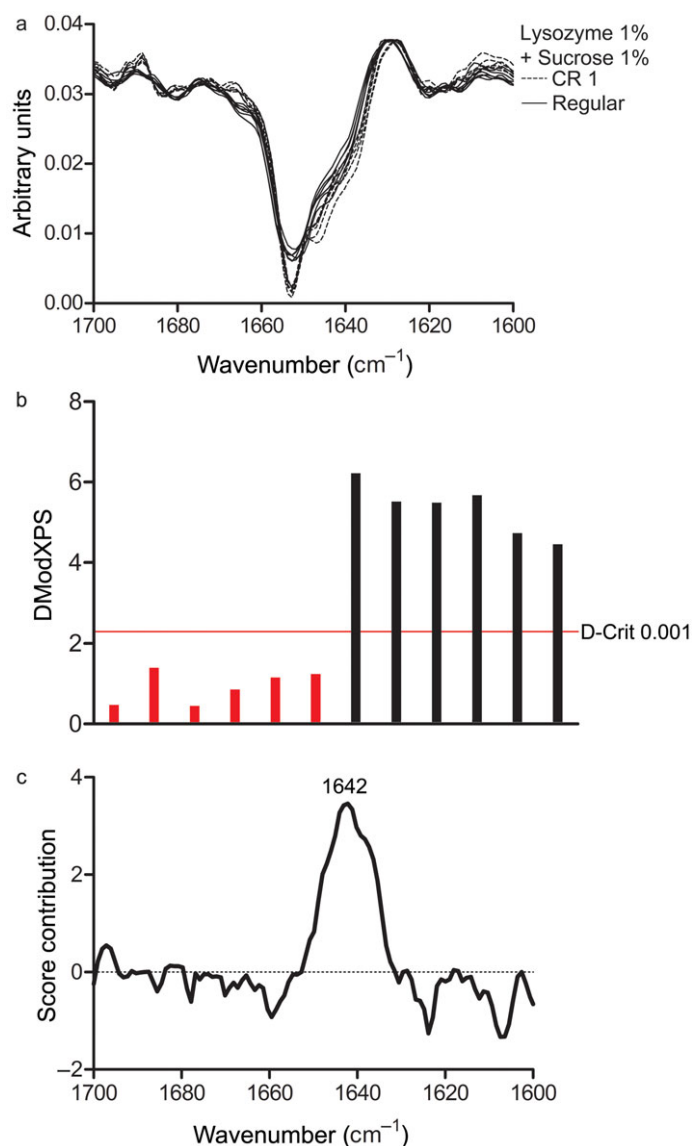


Figure 3. (a) Fourier transformed infrared-ATR spectra of regular MS and MS CR 1 lysozyme 1% + sucrose 1% samples (all w/w). (b) DModXPS distance plot based on a SIMCA-PCA model of regular MS samples prepared from 1% sucrose (w/w; shown as red bars). (c) Contribution plot displaying the main FTIR-ATR band responsible for sample separation. (The reader is referred to the web version of this article for interpretation of the references to color in this figure legend).

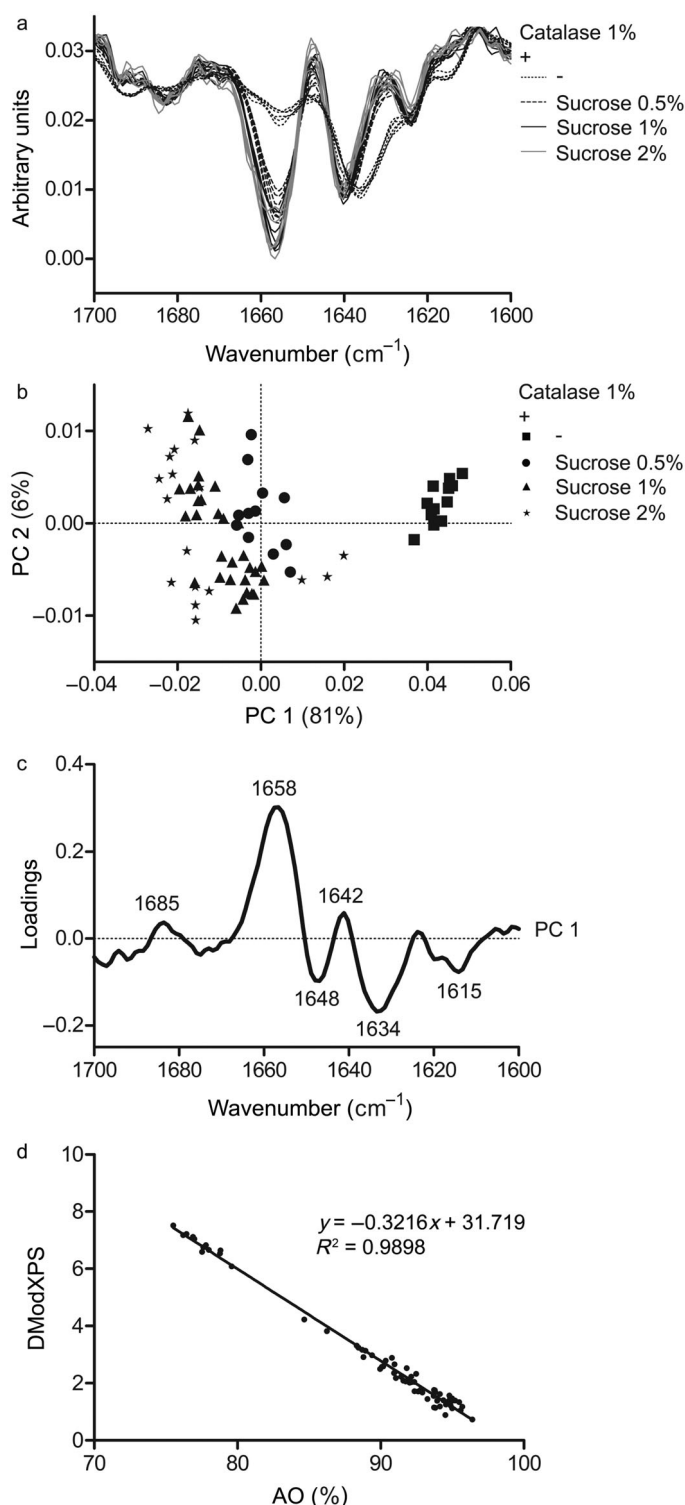


Figure 4. (a) Fourier transformed infrared-ATR spectra of PS catalase samples. (b) PCA score plot of all FTIR-ATR catalase spectra. (c) PCA loading plot of PC 1 to (b). (d) Correlation plot between AO and DModXPS.

As reported in Table 1, for catalase without sucrose, the AO varied between approximately 77%–78%. At a sucrose–catalase ratio of 0.5, the AO increased to approximately 89%–92%, at a ratio of 1 to approximately 91%–95%, and achieved approximately 94%–96% at a ratio of 2 excluding the PS AN 10 bottom

samples, which revealed a strongly reduced AO of 87%. All of the sucrose 1% and 2% samples displayed a tendency toward greater AO at the top when comparing bottom and top against their respective references (Table 1, columns “Bottom Versus Bottom” and “Top Versus Top”). The results of the SIMCA model created from MS and PS regular bottom sucrose 1% and 2% samples are presented in Figure 6. Representative FTIR-ATR spectra of PS samples in Figure 6a provide an overview of the sample location-dependent protein secondary structure variation. The observed peak intensity difference of the α -helical peak at approximately 1656 cm^{-1} and disordered structures at approximately 1648 cm^{-1} agreed well with the contribution plot (Fig. 6c). Interestingly, although all MS top samples were considered to belong to the model sample group, two out of three PS regular sucrose 1% and all PS regular sucrose 2% samples did not belong to the model sample group (Fig. 6b, model samples shown as red bars). In an attempt to provide evidence for the relation between initial filling height, ice crystal morphology, and protein secondary structure, the DModXPS descriptor was plotted against the initial filling height (Fig. 6d) and ice crystal mean size modeled for a mannitol formulation at a T_n of -14°C as conducted by Nakagawa et al.²² (Fig. 6e).

The biological activity of samples reconstituted immediately after freeze-drying is displayed in Figure 7. Catalase without sucrose underwent a drastic biological activity loss when prepared either with MS (Fig. 7a) or with PS (Fig. 7b) equipment. All formulations containing sucrose displayed no major differences in biological activity.

Catalase Formulations—Aggressive Annealing

As mentioned before, MS AN 10 samples collapsed during processing and therefore these samples were not available for further investigation. Assuming that annealing would cause similar morphological effects, irrespective of whether freeze-dried at MS or PS, one PS AN 10 sample and two control samples, one PS regular and one PS AN 20, were prepared at a sucrose–catalase ratio of 1 and investigated by SEM. Representative surface areas of one PS regular, PS AN 20, and PS AN 10 sample are presented in Figure 8. Regular processed samples were found with either round or slit pores (Fig. 8 a-I). A decreasing number of pores was found as the annealing temperature was increased (Figs. 8 b-I and 8c-I). Images taken from the side of the respective samples revealed a thickness of approximately $1.0\text{--}1.1\ \mu$ for all samples (Figs. 8 a-II–8c-II). Additional SEM images confirming that none of the morphological variations were caused by the sample coating process are available in the supplementary material.

DISCUSSION

Equipment Scale and Process Cycle Differences

Differences in the MS and PS processes (i.e., differences in sample placement, target cooling temperature, chamber pressure, and secondary drying temperature) will be considered before the MS and PS results are compared. At PS, vials were placed in the center of the middle shelf surrounded by three rows of dummy vials filled with water to ensure consistent heat transfer. Because of the distance of the shelf center from the PS freeze-dryer Plexiglas door, it was anticipated that there would be reduced radiative heat transfer. The curved vial bottom shape provides little direct contact between vial and shelf,²³

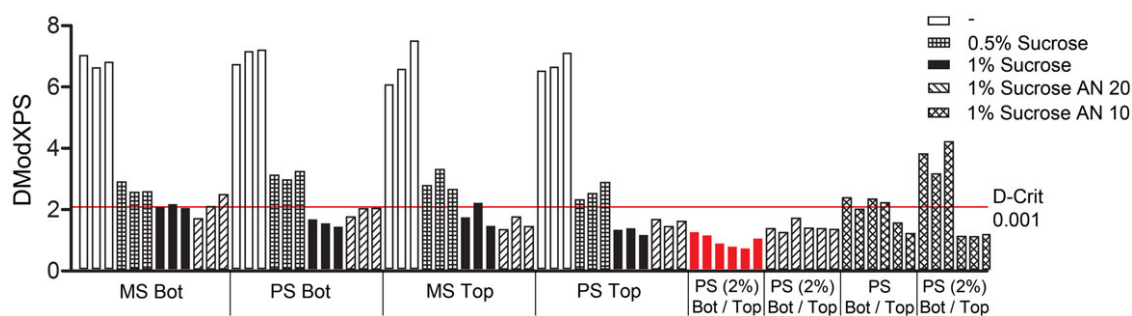


Figure 5. Catalase DModXPS distance plot based on the SIMCA-PCA model of PS samples prepared from 2% sucrose (all w/w; shown as red bars). (The reader is referred to the web version of this article for interpretation of the references to color in this figure legend).

but the gas-filled gap may have influenced the heat transfer characteristics depending on the chamber pressure.²⁴ In the MS approach, the silver heating stage was utilized as a shelf but no space was available in which to place surrounding dummy samples. As the MS freeze-drying cell originates from a microscopy assembly, there was a window directly above the sample. Thus, it appeared reasonable to assume that radiative heat transfer would be a major contributor to the total heat transfer. No gap was present below the sample because of the silicon oil and the plane sample holder bottom. Therefore, the sample container was in direct contact with the shelf. Although these differences were anticipated to influence the overall heat transfer characteristics and subsequently to alter the cycle duration, they were not expected to exert any impact on protein secondary structures. Because of the presumably high radiative heat transfer, the MS target cooling temperature was set at 5°C lower than the respective PS temperature.

The differences in chamber pressure at equal pressure set points resulted from technical limitations and are predicted to have only a minor, if any, influence on MS heat transfer, as there was no gap between the bottom of the sample container and the shelf. Furthermore, this effect was considered more likely to influence the cycle duration than to alter protein secondary structures.

The 5°C difference in secondary drying temperature was related to the volume of the liquid nitrogen reservoir. At 30°C, the liquid nitrogen flow rate is minimal, which reduces the risk of running out of liquid nitrogen but ensures that earlier sublimed ice remains frozen close to the nitrogen inflow port that acts as the condenser. Importantly, no collapse was noted while approaching the secondary drying temperature, and the secondary drying temperatures were well below the glass transition temperatures of sucrose–lysozyme²⁵ and sucrose–catalase formulations,²⁶ both reported to be between 60°C and 70°C at low residual moisture levels. Here, samples revealed a residual moisture content of less than 0.5% (v/v), so that the secondary drying target temperatures were predicted to have only a minor, if any, influence on protein secondary structures.

Regular Process Cycle Results—Are MS and PS Equivalent?

The AO calculation, PCA, and SIMCA modeling of the FTIR-ATR all confirmed the ability of the disaccharide, sucrose, to stabilize both model proteins and are in good agreement with earlier reports for lysozyme^{5,26} and catalase.²⁶ The protective effect of sucrose was also confirmed by measurement of the post freeze-drying biological activity of catalase; this was drastically reduced when there was no sucrose added but generally well

preserved in the presence of sucrose. In addition, biological activity was not reduced for lysozyme in agreement with earlier assessments of freeze-dried lysozymes' biological activity.^{5,26} However, because of the ability of lysozyme to refold into its biologically active conformation after reconstitution,⁸ this cannot be construed as confirmation of the protective effect of sucrose.

When inspecting Table 1 for differences between MS and PS AO for both lysozyme and catalase, a trend was found; it displayed a decrease of approximately 2%–4% at MS. On the PCA score plots (Figs. 1b 4b), both MS and PS samples were found to group together. However, the assessment of the SIMCA-PCA modeling revealed that several, but not all, of the MS samples matched well with the respective PS model sample groups (Figs. 2 and 5). Given the small sample set ($n = 3$), it may not be possible to draw any firm conclusions on equivalency. Nevertheless, the assessment does indicate that there had been very similar stabilization of secondary structures of these two model proteins with MS and PS vial freeze-drying approaches.

Process Cycle Variations—MS Cooling Rate

With respect to the AO calculations, MS CR 1 samples exhibited no obvious differences to their regular MS counterparts up to a sucrose–lysozyme ratio of 0.5, but revealed a tendency toward structural differences at a ratio of 1. This result was surprising, as the key characteristics of the freezing process such as the T_n (Table 2) and the short duration until full solidification of the sample (visual observation) appeared to be similar, and sucrose is known to remain amorphous throughout the freeze-drying process.²⁷ The main difference to regularly cooled down MS samples was the increased β -sheet content, as revealed in the SIMCA-PCA contribution plot (Fig. 3c). As one can identify an increase in α -helical content and at the same time the increase in β -sheet content is far less than occurred with the lysozyme samples prepared without sucrose, it appears that both MS regular and MS CR 1 samples were similar to the PS model sample group in Figure 2. Although it is not possible to generalize this finding to claim that an increase in ordered protein secondary structures can be achieved at reduced cooling rates, variations because of different cooling rates can be expected. With respect to proteins, the relationship between cooling rate and ice crystal size²² potentially leads to significantly different results, if proteins are prone to surface denaturation at the ice–water interface.²⁸ There is also the contribution of excipients to be considered, for example, mannitol, another common excipient in freeze-drying, is known to display polymorphic variations depending on the cooling rate²⁹ and formulation.³⁰

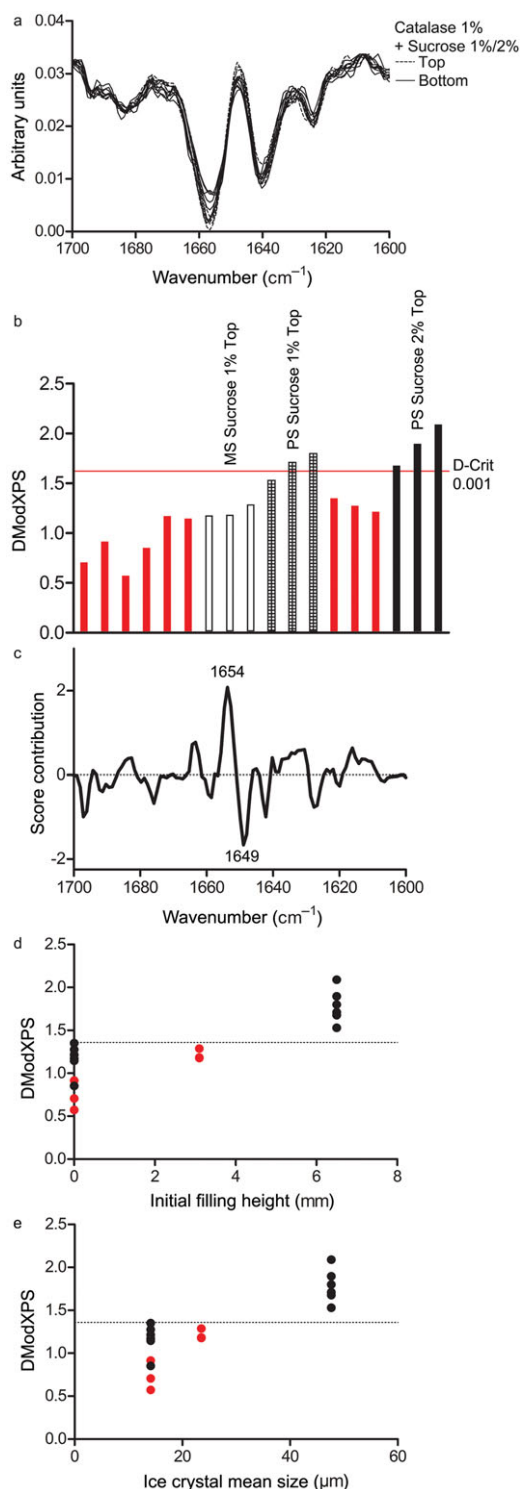


Figure 6. (a) Top and bottom FTIR-ATR spectra of regular PS catalase 1% + sucrose 1%/sucrose 2% samples (all w/w). (b) DModXPS distance plot based on a SIMCA-PCA model of bottom MS and PS samples prepared from 1% and/or 2% sucrose (all w/w; shown as red bars). (c) Contribution plot displaying the main FTIR-ATR bands responsible for sample separation. (d) Correlation plot between initial filling height and DModXPS (MS samples shown as red dots, PS samples shown as black dots). (e) Correlation plot between ice crystal mean size and DModXPS (MS samples shown as red dots, PS samples shown as black dots). (The reader is referred to the web version of this article for interpretation of the references to color in this figure legend).

Process Cycle Variations—Annealing

The annealing step and its effect on cake structure have been claimed previously to allow ice crystals to rearrange, a phenomenon also referred to as Ostwald ripening,³¹ leading to freeze-dried cakes with larger pores than the pores of samples originating from standard freezing protocols.³² Here, annealing durations of 30 min (MS) and 10 h (PS) were chosen to represent a substantial part of the respective total process durations, but no attempt was made to scale the degree of annealing.

At a sucrose–catalase ratio of 1, regular catalase samples were successfully protected as indicated by the similarity to the model sample group in Figure 5. The same was true for MS and PS AN 20 samples, but annealing at -10°C caused collapse at MS, whereas at best minor protein secondary structure differences to the model sample group were noted for PS samples. The annealing temperatures applied here were similar to those commonly reported, ranging from -5°C to -15°C .^{33–37} It has also been stated earlier that in order to achieve a beneficial effect on the primary drying rate, the annealing temperature should exceed a formulation's glass transition temperature of the maximally freeze-concentrated solution (T_g') without causing sample melt.³⁸ The annealing temperatures applied here exceeded the T_g' values of all formulations annealed at MS and PS according to the DSC measurements (Fig. 9). With respect to the lysozyme formulation (Fig. 9a), the measured T_g' was found in between the T_g' values measured for sucrose (1%: -33.36°C , 2%: -33.27°C ; thermograms not shown) and lysozyme (-16.5°C ³⁹), and the catalase formulation T_g' was found to be indistinguishable from sucrose (Fig. 9b), presumably because of the low concentrations and the close T_g' values of sucrose and catalase (-29°C).⁴⁰ Furthermore, no melting was observed during the MS freeze-drying cycle. Although the criteria for annealing were met, SEM images (Fig. 8) provided evidence that there was a reduced number of pores at the surface with increasing annealing temperatures. Therefore, it could be proposed that 30 min annealing at MS drastically reduced the amount of pores in the surface layer of the catalase MS AN 10 samples that increased the resistance to vapor flow, finally resulting in collapse. Considering the increased radiative heat transfer to the sample top mentioned above, it appears possible that the actual annealing temperature at the sample top may have been even higher than that applied to the PS samples used for SEM assessment. The corresponding catalase PS AN 10 samples were similar to the model sample group (Fig. 5), whereas at a sucrose–catalase ratio of 2, PS AN 10 samples revealed a major change in the sample bottom area, that is, there was an AO reduction to 87% (Table 1), a clear separation on the PCA score plot (Fig. 4b), and an apparent distance to the model sample group (Fig. 5). This finding was interpreted to be a consequence of smaller ice crystals at the sample bottom⁵ and the assumption that Ostwald ripening preferably causes rearrangement of small ice crystals,³¹ leading to increased stress on the protein secondary structures present at the bottom. On the basis of the available data, it remains open why perturbation of the protein secondary structures was found clearly increased at the higher sucrose–catalase ratio of 2 but only marginally increased at the ratio of 1.

Interestingly, lysozyme AN 10 samples showed good similarity to the reference samples or model sample group (Table 1; Figs. 1b and 2), irrespective of whether they were prepared with MS or PS equipment. However, it should be remarked

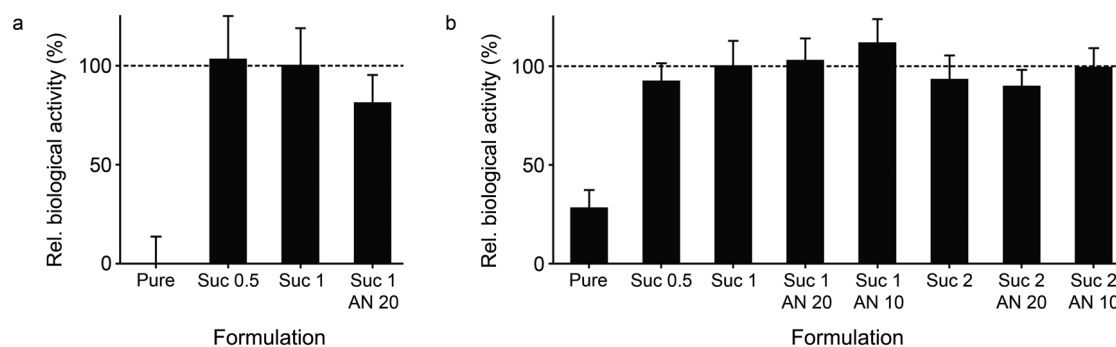


Figure 7. Results of the catalase biological assay normalized to formulation catalase 1% + 1% sucrose (all w/w). Error bars represent standard deviation. All formulations contain 1% catalase (w/w). Abbreviations: Suc 0.5, sucrose 0.5% (w/w); Suc 1, sucrose 1% (w/w); Suc 2, sucrose 2% (w/w); AN 20, Annealing at -20°C ; AN 10, annealing at -10°C . (a) MS results (b) PS results.

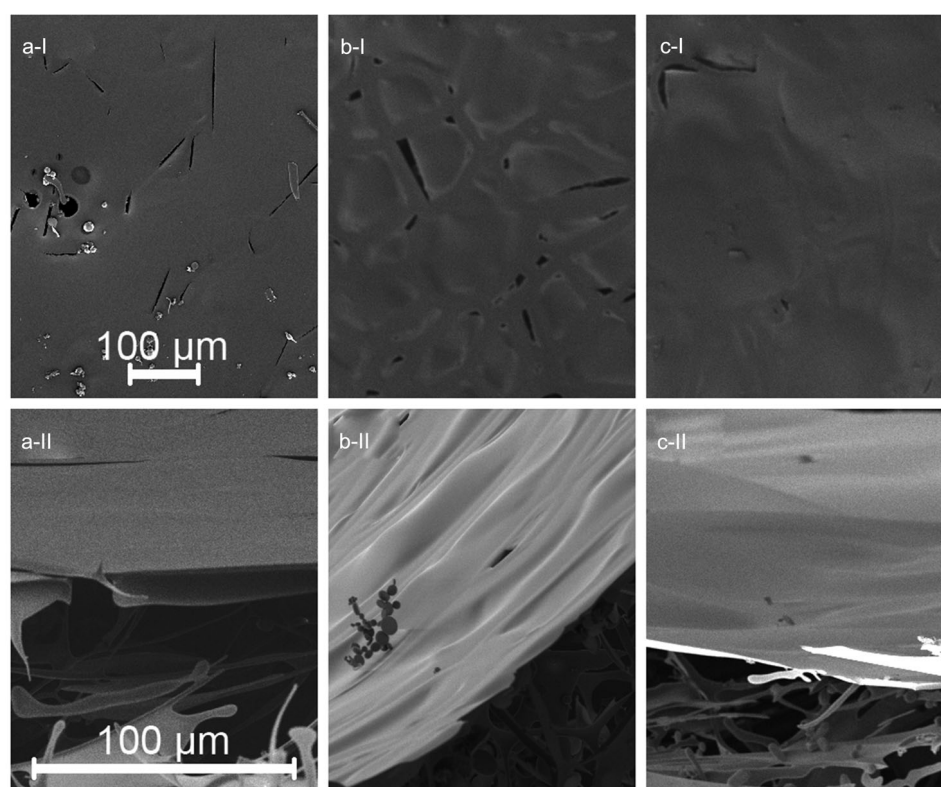


Figure 8. Representative SEM images of PS 1% catalase + 1% sucrose (all w/w) samples. Top row (a-I–c-I): surface image of sample top. Bottom row (a-II–c-II): side view of the surface layer. Scale bars valid for the respective row. Linear contrast and brightness adjustment were performed on complete sections without eliminating, reducing, and/or enhancing any original information present in accordance with ethical guidelines of digital image manipulation. Denotations: a, regular process; b, annealing at -20°C ; c, annealing at -10°C .

that sucrose–lysozyme constitutes a rare case of a specific disaccharide–protein interaction that has been revealed after structural analysis of the high-resolution X-ray experimental data of the lysozyme in 20% sucrose compared with apo protein (Fig. 10). The unique sucrose is located between the α -helical and β -sheet containing regions. The specific intramolecular interactions consist of the direct contacts between hydroxyl moieties of sucrose and five lysozyme residues (aspartate 52, glutamine 57, asparagine 59, tryptophan 63, and alanine 107). In addition, there are four water-mediated hydrogen bonds present in the same structure. Most of the directly mediated hy-

drogen bonds are considered as very strong ones with a length under 3.0 \AA . A possible mechanistic explanation for this interaction is the nature of this enzyme to catalyze the breakage of 1,4- β bonds between N-acetylmuramic acid and N-acetyl-D-glucosamines or between two N-acetyl-D-glucosamines. Here, we hypothesize that sucrose that is bound between the two domains mimics the binding of N-acetyl-D-glucosamine. Nonetheless, it appears reasonable to conclude that one can achieve similar annealing effects on protein secondary structures with both MS and PS, although it may be protein, temperature, duration, and excipient–protein ratio dependent.

Table 2. Model Protein Formulations and MS Nucleation Temperatures of FTIR-ATR Samples (Excluding Annealed Samples)

Formulation		Protocol ^a	MS Nucleation Temperature (°C)		
Protein	Stabilizer		Sample 1	Sample 2	Sample 3
Lysozyme (1%)	–	Regular	–16.5	–15.9	–11.2
		CR 1	–9.6	–18.6	–15.4
	Sucrose (0.5%)	Regular	–18.5	–16.9	–16.5
		CR 1	–16.0	–18.6	–15.4
	Sucrose (1%)	Regular	–16.7	–18.1	–13.9
	CR 1	–11.1	–14.7	–13.0	
Catalase (1%)	–	Regular	–19.8	–17.6	–19.7
	Sucrose (0.5%)	Regular	–17.4	–21.3	–13.7
	Sucrose (1%)	Regular	–17.8	–17.7	–19.5
	Sucrose (2%)	^b	–	–	–

^aRegular protocol cooling rates were 10°C/min for MS and 1°C/min for PS.

^bFormulation prepared in PS only.

All percentages reported as w/w.

CR 1, cooling rate 1°C/min; MS, microscale; PS, pilot scale.

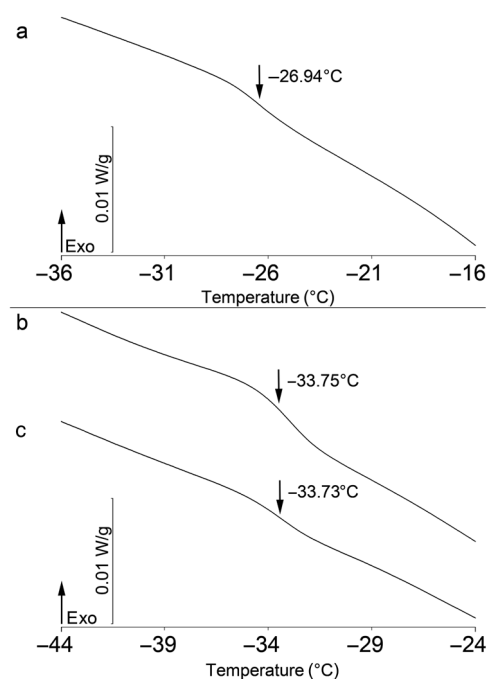


Figure 9. Differential scanning calorimetry thermograms of the formulations utilized for annealing. (a) 1% lysozyme + 1% sucrose (b) 1% catalase + 2% sucrose (c) 1. Catalase + 1% sucrose (all w/w).

Local Sample Variations—Bottom and Top

On the basis of the finding of protein denaturation at the ice–water interface,²⁸ ice crystal growth from bottom to top following nucleation,⁴¹ and the correlation between initial filling height, T_n , and ice crystal morphology,²² it appeared reasonable to conclude that protein secondary structure differences were related to either initial filling height or ice crystal mean size. Considering the initial sample volumes and the inner diameter of the sample containers, the initial filling height was approximately 3.1 mm for MS and 6.5 mm for PS. Although one can argue about the significance of the protein secondary struc-

ture difference (Fig. 6b), a trend was detected for a correlation between DModXPS versus initial filling height (Fig. 6d) and versus ice crystal mean size (Fig. 6e). The ice crystal mean size was taken from a model developed for a 10% mannitol solution at $T_n = -14^\circ\text{C}$ ²² and therefore should only be considered as a rough indicator.

As no local variation was found for lysozyme, it is currently not possible to state whether this result was specific to the investigated catalase formulations or if local variation was greatly reduced for lysozyme because of the rare specific interaction with sucrose, as mentioned above.

CONCLUSIONS

A MS approach was used to freeze-dry two model proteins formulated without stabilizer and in sucrose. This approach resulted in a similar degree of protection of protein secondary structures as could be observed in PS vial freeze-drying samples. The SIMCA-PCA modeling approach was successfully employed in the analysis of solid-state FTIR-ATR spectra and revealed an excellent correlation to the AO parameter. Spectroscopic analysis complemented the post freeze-drying biological activity assessment in determining the similarities between the MS and PS samples, but provided additional insights into the solid-state protein secondary structures. Furthermore, it was possible to relate differences in the protein secondary structures between bottom and top to the initial filling height and the ice crystal mean size. Similar annealing effects were achieved at MS and PS for lysozyme and some catalase formulations at some process cycles indicating the potential to evaluate annealing effects during early-stage formulation development. Nevertheless, a better mechanistic understanding of annealing at both scales would be required to avoid a trial-and-error approach, especially for proteins prone to damage at the ice–water interface and without the possibility of a specific interaction with the stabilizer. There was some evidence for some influence of the cooling rate with MS but further investigations involving other model proteins and excipients will be required to understand the dimension of the cooling rate effect.

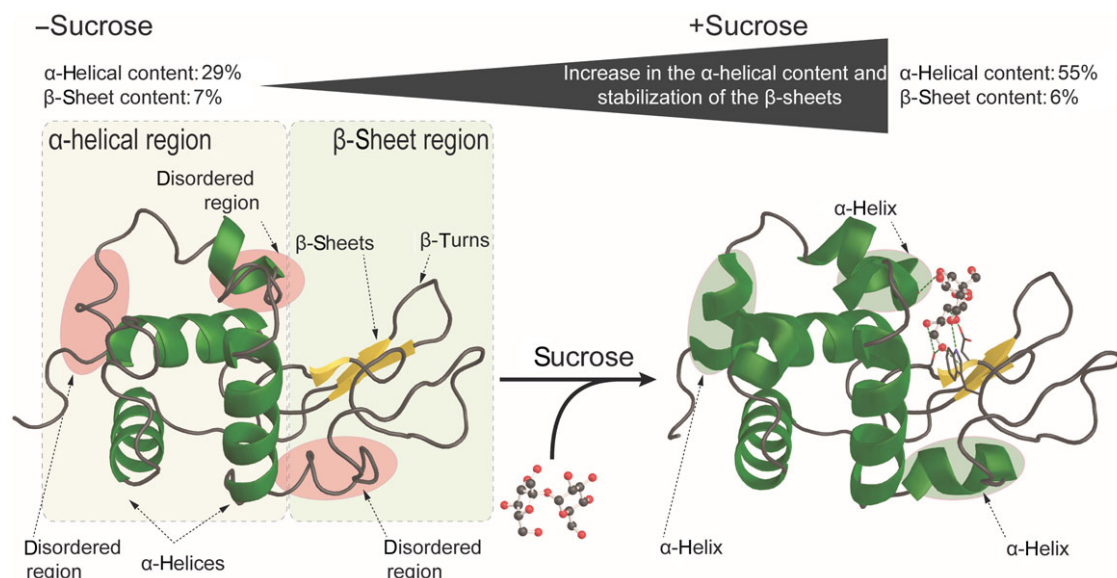


Figure 10. Stabilization of the lysozyme upon sucrose binding. The stabilization of the disordered regions (highlighted with circles) leads to an increase in the α -helical content. The hydrogen bonding network between the sucrose and lysozyme is highlighted with green dashed lines. The α -helical and β -sheet containing regions are bridged together upon sucrose binding stabilizing the protein. The X-ray structure of the lysozyme without sucrose is based on PDBID 132L, whereas lysozyme with 20% sucrose is based on PDBID 3SP3. Visualization and the secondary structure content calculation were conducted with PyMOL (The PyMOL Molecular Graphics System, version 1.7.4 Schrodinger, LLC.). (The reader is referred to the web version of this article for interpretation of the references to color in this figure legend).

ACKNOWLEDGMENTS

The authors gratefully acknowledge the financial support of the FinPharma Doctoral Program and the Orion Farnos Foundation as well as the provision of equipment by the PROMIS Centre consortium (supported by the Finnish Funding Agency for Technology and Innovation (Tekes), the Regional Council of Pohjois-Savo, the North Savo Centre for Economic Development, Transportation and Environment, and participating industrial partners), SIB Labs, and the School of Pharmacy. The authors also thank Pharm. Kristi Markna (University of Tartu, Estonia) for her technical help and Dr. Ewen MacDonald (University of Eastern Finland) for proofreading of the manuscript.

The funding sources had no involvement in study design, collection, analysis, and interpretation of the data, in the writing of the report, and in the decision to submit the article for publication.

The authors declare that no conflict of interest influenced this work.

REFERENCES

- Pikal MJ. 2002. Freeze drying. In *Encyclopedia of pharmaceutical technology*; Swarbrick JS, Boylan JC, Eds. New York: Marcel Dekker, pp 1299–1326.
- Bhatnagar BS, Bogner RH, Pikal MJ. 2007. Protein stability during freezing: Separation of stresses and mechanisms of protein stabilization. *Pharm Dev Technol* 12:505–523.
- Grant Y, Matejtschuk P, Dalby PA. 2009. Rapid optimization of protein freeze-drying formulations using ultra scale-down and factorial design of experiment in microplates. *Biotechnol Bioeng* 104:957–964.
- Trnka H, Wu JX, De Weert MV, Grohganz H, Rantanen J. 2013. Fuzzy logic-based expert system for evaluating cake quality of freeze-dried formulations. *J Pharm Sci* 102:4364–4374.
- Peters B, Molnár F, Ketolainen J. 2014. Structural attributes of model protein formulations prepared by rapid freeze-drying cycles in a microscale heating stage. *Eur J Pharm Biopharm* 87:347–356.
- Grant Y, Matejtschuk P, Bird C, Wadhwa M, Dalby P. 2012. Freeze drying formulation using microscale and design of experiment approaches: A case study using granulocyte colony-stimulating factor. *Biotechnol Lett* 34:641–648.
- Allison SD, Dong A, Carpenter JF. 1996. Counteracting effects of thiocyanate and sucrose on chymotrypsinogen secondary structure and aggregation during freezing, drying, and rehydration. *Biophys J* 71:2022–2032.
- Prestrelski SJ, Arakawa T, Carpenter JF. 1994. Structure of proteins in lyophilized formulations using Fourier transform infrared spectroscopy. In *Formulation and delivery of proteins and peptides*; JL Cleland, R Langer, Eds. Washington, DC: American Chemical Society, pp 148–169.
- Prestrelski SJ, Tedeschi N, Arakawa T, Carpenter JF. 1993. Dehydration-induced conformational transitions in proteins and their inhibition by stabilizers. *Biophys J* 65:661–671.
- International Conference on Harmonisation of Technical Requirements for Registration of Pharmaceuticals for Human Use, August 2009. 2015. ICH harmonised tripartite guideline: Pharmaceutical development Q8 (R2).
- Susi H. 1972. [22] Infrared spectroscopy—Conformation. *Meth Enzymol* 26:455–472.
- Krimm S, Bandekar J. 1986. Vibrational spectroscopy and conformation of peptides, polypeptides, and proteins. *Adv Protein Chem* 38:181–364.
- Dong A, Huang P, Caughey WS. 1990. Protein secondary structures in water from second-derivative amide I infrared spectra. *Biochemistry* 29:3303–3308.
- Dong A, Caughey WS. 1994. [9] Infrared methods for study of hemoglobin reactions and structures. *Meth Enzymol* 232:139–175.
- Stockdale G, Murphy BM, D'Antonio J, Manning MC, Al-Azzam W. 2015. comparability of higher order structure in proteins: Chemometric analysis of second-derivative amide I fourier transform infrared spectra. *J Pharm Sci* 104:25–33.

16. Wang W. 2000. Lyophilization and development of solid protein pharmaceuticals. *Int J Pharm* 203:1–60.
17. Heljo V, Jouppila K, Hatanpää T, Juppo A. 2011. The use of disaccharides in inhibiting enzymatic activity loss and secondary structure changes in freeze-dried β -galactosidase during storage. *Pharm Res* 28:540–552.
18. Carpenter JF, Crowe JH. 1989. An infrared spectroscopic study of the interactions of carbohydrates with dried proteins. *Biochemistry* 28:3916–3922.
19. Meyer JD, Manning MC, Carpenter JF. 2004. Effects of potassium bromide disk formation on the infrared spectra of dried model proteins. *J Pharm Sci* 93:496–506.
20. Luthra S, Kalonia DS, Pikal MJ. 2007. Effect of hydration on the secondary structure of lyophilized proteins as measured by Fourier transform infrared (FTIR) spectroscopy. *J Pharm Sci* 96:2910–2921.
21. Kendrick BS, Dong A, Allison SD, Manning MC, Carpenter JF. 1996. Quantitation of the area of overlap between second-derivative amide I infrared spectra to determine the structural similarity of a protein in different states. *J Pharm Sci* 85:155–158.
22. Nakagawa K, Hottot A, Vessot S, Andrieu J. 2007. Modeling of freezing step during freeze-drying of drugs in vials. *AIChE J* 53:1362–1372.
23. Hibler S, Wagner C, Gieseler H. 2012. Vial freeze-drying, part 1: New insights into heat transfer characteristics of tubing and molded vials. *J Pharm Sci* 101:1189–1201.
24. Ganguly A, Nail SL, Alexeenko A. 2013. Experimental determination of the key heat transfer mechanisms in pharmaceutical freeze-drying. *J Pharm Sci* 102:1610–1625.
25. Liao Y, Brown MB, Martin GP. 2004. Investigation of the stabilisation of freeze-dried lysozyme and the physical properties of the formulations. *Eur J Pharm Biopharm* 58:15–24.
26. Liao Y, Brown M, Quader A, Martin G. 2002. Protective mechanism of stabilizing excipients against dehydration in the freeze-drying of proteins. *Pharm Res* 19:1854–1861.
27. Izutsu K, Kojima S. 2002. Excipient crystallinity and its protein-structure-stabilizing effect during freeze-drying. *J Pharm Pharmacol* 54:1033–1039.
28. Chang BS, Kendrick BS, Carpenter JF. 1996. Surface-induced denaturation of proteins during freezing and its inhibition by surfactants. *J Pharm Sci* 85:1325–1330.
29. Kauppinen A, Toiviainen M, Aaltonen J, Korhonen O, Järvinen K, Juuti M, Pellinen R, Ketolainen J. 2013. Microscale freeze-drying with Raman spectroscopy as a tool for process development. *Anal Chem* 85:2109–2116.
30. Larsen HML, Trnka H, Grohgan H. 2014. Formation of mannitol hemihydrate in freeze-dried protein formulations—A design of experiment approach. *Int J Pharm* 460:45–52.
31. Patel S, Bhugra C, Pikal M. 2009. Reduced pressure ice fog technique for controlled ice nucleation during freeze-drying. *AAPS Pharm-SciTech* 10:1406–1411.
32. Patapoff TW, Overcashier DE. 2002. The importance of freezing on lyophilization cycle development. *Biopharm Int* 15:16–21.
33. Heller MC, Carpenter JF, Randolph TW. 1997. Manipulation of lyophilization-induced phase separation: implications for pharmaceutical proteins. *Biotechnol Prog* 13:590–596.
34. Abdul-Fattah AM, Truong-Le V, Yee L, Nguyen L, Kalonia DS, Cicerone MT, Pikal MJ. 2007. Drying-induced variations in physicochemical properties of amorphous pharmaceuticals and their impact on stability (I): Stability of a monoclonal antibody. *J Pharm Sci* 96:1983–2008.
35. Sarciaux J, Mansour S, Hageman MJ, Nail SL. 1999. Effects of buffer composition and processing conditions on aggregation of bovine IgG during freeze-drying. *J Pharm Sci* 88:1354–1361.
36. Webb SD, Cleland JL, Carpenter JF, Randolph TW. 2003. Effects of annealing lyophilized and spray-lyophilized formulations of recombinant human interferon- γ . *J Pharm Sci* 92:715–729.
37. Lueckel B, Helk B, Bodmer D, Leuenberger H. 1998. Effects of formulation and process variables on the aggregation of freeze-dried interleukin-6 (IL-6) after lyophilization and on storage. *Pharm Dev Technol* 3:337–346.
38. Searles JA, Carpenter JF, Randolph TW. 2001. Annealing to optimize the primary drying rate, reduce freezing-induced drying rate heterogeneity, and determine T_g' in pharmaceutical lyophilization. *J Pharm Sci* 90:872–887.
39. Slade L, Levine H, Finley JW. 1989. Protein-water interactions: water as a plasticizer of gluten and other protein polymers. In *Protein quality and the effects of processing*; Philips RD, Finley JW, Eds. New York: Marcel Dekker, pp 9–124.
40. Jiang S, Nail SL. 1998. Effect of process conditions on recovery of protein activity after freezing and freeze-drying. *Eur J Pharm Biopharm* 45:249–257.
41. Searles JA, Carpenter JF, Randolph TW. 2001. The ice nucleation temperature determines the primary drying rate of lyophilization for samples frozen on a temperature-controlled shelf. *J Pharm Sci* 90:860–871.